UNIVERSITY OF CALIFORNIA, SAN DIEGO

Excitons in Transition Metal Dichalcogenide van der Waals Heterostructures

A dissertation submitted in partial satisfaction of the
requirements for the degree
Doctor of Philosophy

in

Physics

by

Erica Calman

Committee in charge:

Professor Leonid Butov, Chair
Professor Ertugrul Cubukcu
Professor Michael Fogler
Professor Charles Tu
Professor Congjun Wu

2019

The dissertation of Erica Calman is approved, and it is acceptable in quality and form for publication on microfilm and electronically:

_____

_____

_____

_____

_____

Chair

University of California, San Diego

2019

EPIGRAPH

I was going to engineering school but fell in love with physics.

Leonard Susskind—

TABLE OF CONTENTS

LIST OF FIGURES

LIST OF TABLES

ACKNOWLEDGEMENTS

I would like to acknowledge my research group, without whom none of this work would have ever begun. I would like to thank my early coworkers Mikas Remeika, Jason Leonard, and Yuliya Kuznetsova. The training and guidance they provided made it possible for me to do anything, and their continuing guidance has helped me on countless occasions. I would like to thank my long running coworkers, Chelsey Dorow and Matthew Hasling for their extensive assistance as well as for providing a work environment that was friendly and which made it possible to get out of bed everyday. I would also like to thank Sergei Potalvstev and Peristera Andreakou for the time they spent at UC San Diego helping to train me. I would like to thank Sheng Hu and the national graphene institute for providing the heterostructures I used as well as for hosting me and teaching me about van der Waals heterostructure fabrication.

I would like to acknowledge the tremendous intellectual support I've received from outside of the Butov group. My family has always supported my intellectual enrichment. I would also like to thank Alexander Kuczala for countless hours of discussion and support.

Finally, I would like to Acknowledge my advisor, Leonid Butov. His patience and dedication have provided me with the guidance and environment I needed to complete this work.

The text of chapter 2, in part, is a reprint of the material as it appears in E. V. Calman, C. J. Dorow, M. M. Fogler, L. V. Butov, S. Hu, A. Mishchenko, A. K. Geim. Control of excitons in multi-layer van der Waals heterostructures, Appl. Phys. Lett. 108, 101901 (2016) © 2016, where the dissertation author was the first author. The co-authors in these publications directed, supervised, and co-worked on the research which forms the basis of this chapter.

The text of chapter 3, in part, is a reprint of the material as it appears in E.V. Calman, M.M. Fogler, L.V. Butov, S. Hu, A. Mishchenko, A.K. Geim. Indirect excitons in van der Waals heterostructures at room temperature, Nature Commun. 9, 1895 (2018). © 2018, where the dissertation author was the first author. The co-authors in these publications directed, supervised, and co-worked on the research which forms the basis of this chapter.

VITA

2012	B. S. in Physics, University of California, Davis
2012-2013	Teaching Assistant, University of California, San Diego
2013-2019	Graduate Research Assistant, University of California, San Diego
20019	Ph. D. in Physics, University of California, San Diego

PUBLICATIONS

E. V. Calman, C. J. Dorow, M. M. Fogler, L. V. Butov, S. Hu, A. Mishchenko, A. K. Geim. Control of excitons in multi-layer van der Waals heterostructures, Appl. Phys. Lett. 108, 101901 (2016)

E. V. Calman, M.M. Fogler, L.V. Butov, S. Hu, A. Mishchenko, A.K. Geim. Indirect excitons in van der Waals heterostructures at room temperature, Nature Commun. 9, 1895 (2018).

P. Andreakou, S.V. Poltavtsev, J.R. Leonard, **E. V. Calman**, M. Remeika, Y. Y. Kuznetsova, L.V. Butov, J. Wilkes, M. Hanson, A.C. Gossard. Optically controlled excitonic transistor, Appl. Phys. Lett. 104, 091101 (2014).

C. J. Dorow, M. W. Hasling, **E. V. Calman**, L. V. Butov, J. Wilkes, K. L. Campman, and A. C. Gossard. Spatially and time-resolved imaging of transport of indirect excitons in high magnetic fields, Phys. Rev. B 95, 235308 (2017).

Y. Y. Kuznetsova, C. J. Dorow, **E. V. Calman**, L. V. Butov, J. Wilkes, K. L. Campman, and A. C. Gossard. Transport of indirect excitons in high magnetic fields, Phys. Rev. B 95, 125304 (2017).

Y. Y. Kuznetsova, F. Fedichkin, P. Andreakou, **E. V. Calman**, L. V. Butov, P. Lefebvre, T. Bretagnon, T. Guillet, M. Vladimirova, C. Morhain, and J.M. Chauveau. Transport of indirect excitons in ZnO quantum wells, Opt. Lett. 40 (15), 3667-3670 (2015).

Y. Y. Kuznetsova, P. Andreakou, M.W. Hasling, J.R. Leonard, **E. V. Calman**, L.V. Butov, M. Hanson, A.C. Gossard. Two-dimensional snowflake trap for indirect excitons, Opt. Lett. 40, 589 (2015).

M.W. Hasling, Y. Y. Kuznetsova, P. Andreakou, J.R. Leonard, **E. V. Calman**, C.J. Dorow, L.V. Butov, M. Hanson, A.C. Gossard. Stirring potential for indirect excitons, J. Appl. Phys. 117, 023108 (2015).

ABSTRACT OF THE DISSERTATION

Excitons in Transition Metal Dichalcogenide van der Waals Heterostructures

by

Erica Calman

Doctor of Philosophy in Physics

University of California, San Diego, 2019

Professor Leonid Butov, Chair

Excitons are quasi-partciles consisting of an electro-statically bound electron and hole which have long been observed in semiconducting and insulating materials. A spatially indirect exciton (IX) is an exciton in which the electron and the hole are spatially separated. This is achieved through the use of a static electric field and engineered semiconductor heterosteructures. Indirect excitons interact with one another and can effeciently re-radiate, so they provide a means for light to interact with light in solid media, and can thus be used for efficient optical signal processing. However, the most common material for studying indirect excitons (GaAs) cannot support excitons at temperatures above $\sim$ 100 K. This limitation, due to thermal fluctuations having enough energy to cause exciton dissocation prevents the creation of practical devices for

excitonic signal processing. This dissertation demonstrates an increase in the binding energy and thus operating temperature of indirect excitons by utelizing van der Waals transition metal dichalcogenide heterostructures. These atomically thin materials have binding energies on the order of 0.5 eV which support excitons at 300 K.

Chapter 1

Introduction

1.1 Indirect Excitons

An exciton is a long-lived quasi-particle excitation of an insulator in which the electron is electrostatically bound and spatially localized around a hole. In every insulator (and thus semiconductor) the lowest energy excitation across the band gap is not the creation of a free electron (and thus free hole), but the creation of an exciton. Excitons have smaller energies than that of the band gap due to the electro-static interation between the electron and the hole which are pair created together [1]. In the ground state, excitons have binding energy $B.E. \sim \frac{\mu e^4}{2h^2\varepsilon^2}$ where the reduced mass $\mu = \frac{m_e m_h}{m_e + m_h}$, and a_B is excitonic Bohn radius. Thus, the binding energy depends on dielectric constant and the effective mass for all excitons. An indirect exciton (IX) is an exciton which has a spatial separation between the electron and the hole. The expression is more complex for indirect excitons as it depends on the construction of the heterostructure. However, it shares the same dependence on effective mass and dielectric constant. The ground state of an indirect exciton however, has a spatial separation between the electron and hole which preclude an analytical solution of the Schr$\acute{}$odinger equation [2].

In the absence of an external electric field, indirect excitons generally have smaller

binding energies (and thus higher total energy) than direct excitons because of the attractive columb interaction between the electron and the hole. However, indirect excitons have a stong first order response to an external electric field (external only in the sense that is not due to the presence of the electron or hole), whereas direct excitons (DX) do not. There is a small degree of level repulsion which prevents a crossing of the IX and DX energy levels. We refer to the direct and indirect regimes of applied gate voltage as the two possible domains. In the direct regime, the reduction in IX energy due to the external electric field is less than the initial offset in binding energy, so the direct exciton is energetically favorable. In the indirect regime, the energy reduction due to voltage overcomes the offset, and the indirect exciton becomes energetically favorable.

Because indirect excitons have large spatial separations between the electron and the hole, their lifetimes are long. This is due to the small overlap in their wavefunctions. In heterostructures with a barrier between the electron and hole, this is overlap is further reduced. This long lifetime facilitates cooling to the lattice temperature, creating studiable cold, dense exciton quantum gasses. These gasses can be manipulated classically using optical excitation [3], applied electric field [4], magnetic field [5, 6] For sufficiently cold lattice temperatures, the gas can also form a condensed superfluid due to being composite bosons of spin 2 and charge 0.

The current technology utilizes GaAs/AlGaAs heterostrcutures to achieve operating temperatures that are typically around $2K$. This requires hours of work and delicate equipment which must be maintained in order to achieve even a classical gas of indirect excitons. Superfluids and superconductors also traditionally require cryogenic cooling to at least the temperature of liquid nitrogen. Utilizing indirect excitons, optical signal proscessing and superfluids might be possible at room temperature.

1.2 Unconventional Materials

Indirect excitons exist in when the binding energy is greater than the thermal excitations of the system, $T < \frac{E_b}{k_b}$. In order to facilitate the operation of devices at practical temperatures (either the 77K of liquid nitrogen or ideally room temperature), a larger binding energy is needed. This can be achieved by decreasing the spatial separation between layers, by decreasing the dielectric constant, or by increasing the effective mass. Traditional GaAs/AlGaAs heterostructures can achieve temperatures of up to $100\ K$ utilizing type II band alignments, but cannot achieve higher operating temperatures. A number of materials have been utilized including ZnO [7], GaN,[8, 9]. These all rely on a combination of band gap engineering and dielectric environment to produce exciton binding energies and Bohrs radii that can keep excitons stable at room temperature.

In addition, traditional materials have to be grown in large, expensive molecular beam epitaxy machines. By contrast, van der Waals heterostrucutures (including transition metal dichalcogenide van der waals structures) only require mechanical exfoliation [10]. These structures can also capitalize on the passivating effects of boron nitride to chemically isolate the quantum wells, providing addition robustness to the environment.

1.3 High Temperature Superfluidity

Excitons are composite bosons of spin 1 or 2. As a result, when they cool below their transition temperature of $T_d = \frac{2\pi\hbar^2}{m_x} n_x$ excitons can form a superfluid state. This is limited by their density. This is because for in plane densitities greater than the bohr radius $r_B = \frac{\hbar^2 \varepsilon}{\mu e^2}$, the exciton gas can break down to form a electron-hole plasma. TMD materials avoid this by having large effective masses and small (for a semiconductor) dielectric constants. Because the effective mass also decreases the transition temperatures, this means transition metal dichalcogenides are ideally suited to the creation of high temperature quantum degenerate gasses.

1.4 Time resolved spectroscopy

The presented work relies on the ability to determine the time dependent behavior of the sample. This primarily consists of measuring the lifetime of the photoluminescence. The separation of the photoluminescence based on wavelength and time yields information about the energy and lifetime of excitons and other quasi-particle excitations in a system. This is achieved utilizing either a time-correlated photon counting system or a gated intensifier. In the case of the time correlated photon counting system spatial information is unavailable. Instead, these measurements are averaged over some small region utilizing and outlet slit for the spectrometer. However, because the detector is a photomultiplier rather than a charge coupled device the sensitivity is much greater. A pulse generator drives a semiconductor laser (for all non-resonant excitations a 404 nm diode was used), which in turn excited the sample. The photoluminescence then passes into the spectrometer inlet, is separated on wavelength via the spectrometer grating, and then reaches the photomultiplier tube or CCD. In the case of the CCD, the light is passed through a gated intensifier which set the time-integration window and is then measured directly by the CCD. In the case of the photomultiplier the signal passed through the time correlated photon counting system. A synchronized start pulse is sent when the laser pulse begins, and a time to analogue converter is used to produce a voltage corresponding to the delay between the start signal from the and the stop signal from the PMT. These voltages are then sent as an output pulse of fixed duration which is read by an analogue to digital converter and counted in software.

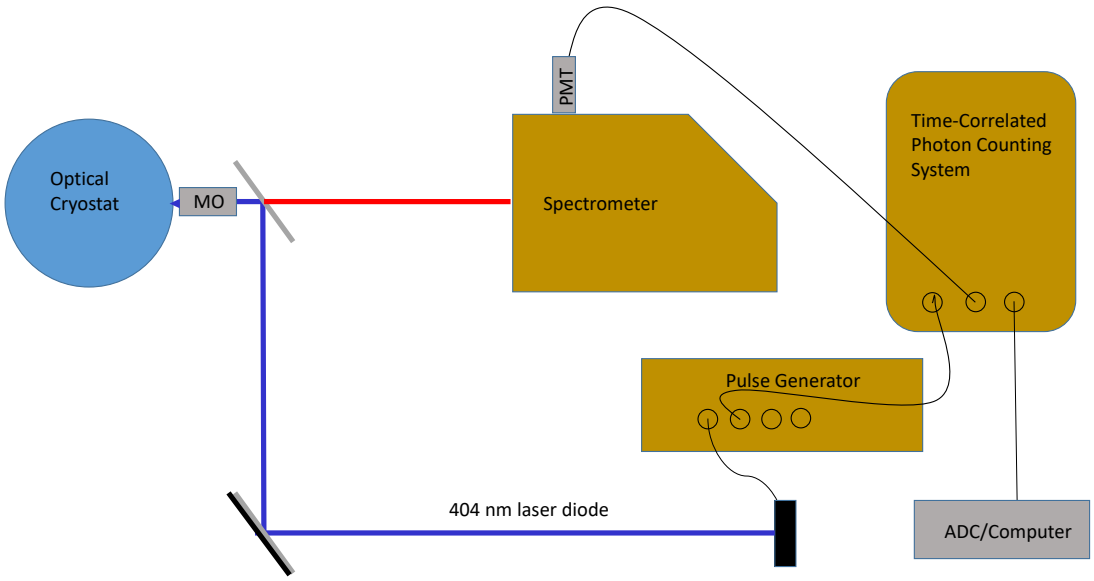

Figure 1.1: The time resolved setup showing the optical path (blue/red lines for excitation/signal respestively)

1.5 TMD device fabrication

TMD devices were prepared via the famous ”scotch tape” method of mechanical exfoliation. Low residue tape is used to separate thin pieces of TMD material from the bulk crystal. These pieces ar then reduced to single or few layer thicknesses by adhering the tape to the top layer and removing it until the desired thickness is achieved (usually an atomically thin monolayer). This is done on a film of polymer so that that the piece of material can be transfered to the existing structure. These are then transfered to a substrate one at a time in order to create a van der Waals heterostructure.

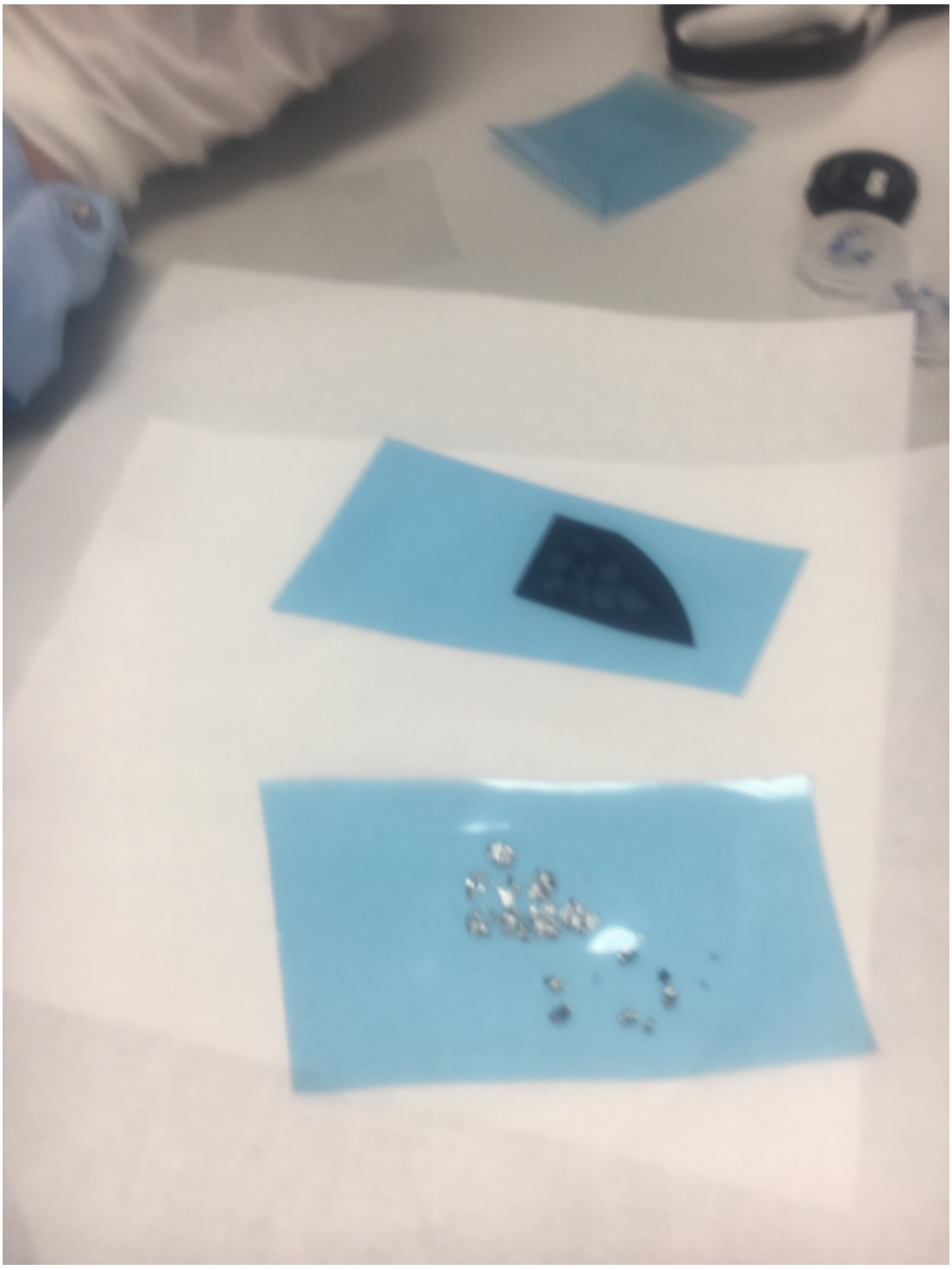

Figure 1.2: The unexfoliated layers of TMD attached to low resigue tape (foreground) and in the process of being adhered to a substrate for exfoliation

Chapter 2

Trions and Direct Excitons in TMD

In this chapter we report an experimental study of excitons in a double quantum well van der Waals heterostructure made of atomically thin layers of MoS_2 and hexagonal boron nitride (hBN). The emission of neutral and charged excitons is controlled by gate voltage, temperature, and both the helicity and the power of optical excitation.

2.1 Introduction to Trions and Direct Excitons in TMD

Van der Waals heterostructures composed of ultrathin layers of transition metal dichalcogenides (TMD), such as MoS_2, WSe_2, etc., offer an opportunity to realize artificial materials with designable properties, forming a new platform for studying basic phenomena and developing optoelectronic devices [10]. In TMD structures, excitons have high binding energies and are prominent in the optical response. The energy, intensity, and polarization of exciton emission gives information about electronic, spin, and valley properties of TMD materials [11, 12, 13, 14, 15, 16, 17, 18, 19, 20, 21, 22, 23, 24, 25, 26, 27, 28, 29, 30, 31, 32].

Exciton phenomena are expected to become even richer in structures that contain two 2D layers. The energy-band diagram of such a coupled quantum well (CQW) structure is shown schematically in Figure 1b. Previous studies of GaAs [33], AlAs [34], and InGaAs [35]

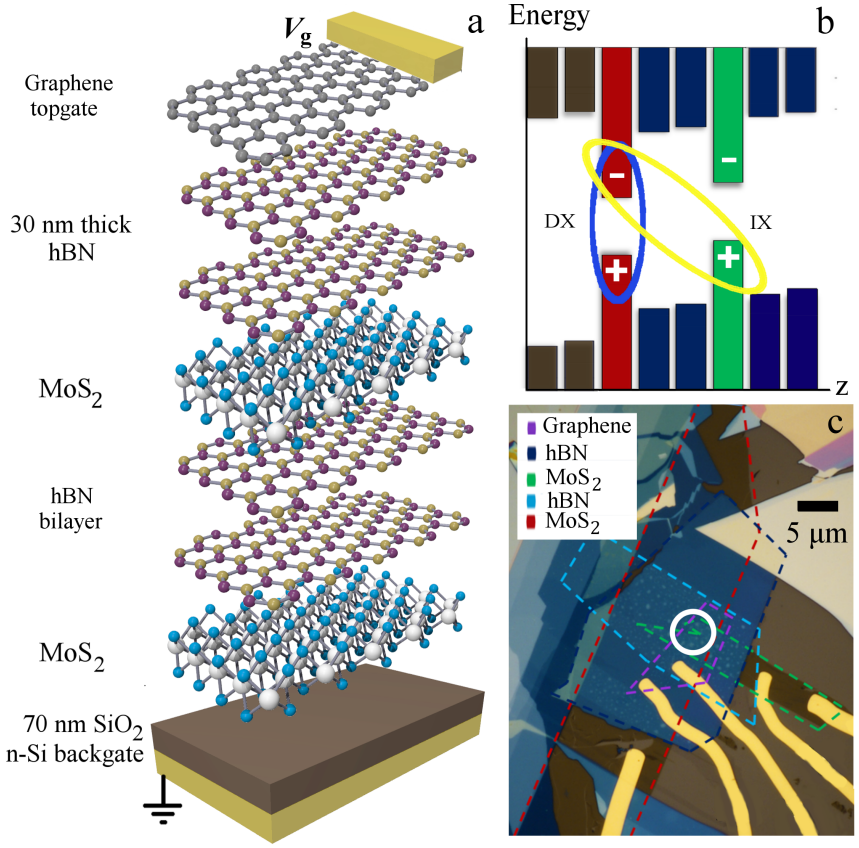

Figure 2.1: The coupled quantum well van der Waals heterostructure. Layer (a) and energy-band (b) diagrams. The ovals indicate a direct exciton (DX) and an indirect exciton (IX) composed of an electron (−) and a hole (+). (c) Microscope image showing the layer pattern of the device. The position of the laser excitation spot is indicated by the circle.

CQWs showed that excitons in these structures can be effectively controlled by voltage and light. Two types of excitons are possible in a CQW structure. Spatially direct excitons (DXs) are composed of electrons and holes in the same layer, while indirect excitons (IXs) are bound states of electrons and holes in the different layers separated by a distance d, Figure 1b. IXs can form quantum degenerate Bose gases [36, 37]. The realization and control of quantum IX gases was demonstrated [38, 39] in GaAs CQW structures at temperatures T below a few degrees Kelvin. In a recent theoretical work [40] it was predicted that the large exciton binding energies in TMD CQW structures may bring the domain of these phenomena to high temperatures. On the other hand, DXs in TMD CQW structures have a high oscillator strength making these structures good

emitters [11, 12, 13, 14, 15, 16, 17, 18, 19, 20, 21, 22, 23, 24, 25, 26, 27, 28, 29, 30, 31, 32]. CQW structures allow control of the exciton emission by voltage. These properties make CQW structures an interesting new system for studying exciton phenomena in TMD materials.

The DX binding energy E_{DX} is larger [40] than that E_{IX} of the IXs, so in the absence of an external field the DXs are lower in energy. The electric field F normal to the layers induces the energy shift eFd of IXs. The transition between the direct regime where DXs are lower in energy to the indirect regime where IXs are lower in energy occurs when $eFd > E_{\mathrm{DX}} - E_{\mathrm{IX}}$ [35]. Both direct and indirect regimes show interesting exciton phenomena. The indirect regime was considered in earlier studies of GaAs [33], AlAs [34], InGaAs [35], and TMD [27, 30] CQW structures. The direct regime in TMD CQW structures is considered in this work. Exploring the direct regime is essential for understanding both the universal properties of complex exciton systems in CQW structures and the specific properties of direct excitons in TMD layers We found that the exciton spectra in the direct regime have three exciton emission lines. The ability to control the CQW structure by voltage provides an important tool for understanding the complex exciton emission in TMD structures. The measured dependence of exciton spectra on voltage, temperature and excitation indicated that the lines correspond to the emission to neutral and charged excitons.

The structure studied here was assembled by stacking mechanically exfoliated layers on a Si/SiO_2 substrate, which acts as a global backgate (Figure 1a). The top view of the device showing the contours of different layers is presented in Figure 1c. The CQW is formed where the two MoS_2 monolayers, separated by an hBN bilayer, overlap. The upper 20–30 nm thick hBN served as a dielectric cladding layer for a top graphene electrode. Voltage V_g applied between the top graphene layer and a backgate was used to create the bias across the CQW structure.

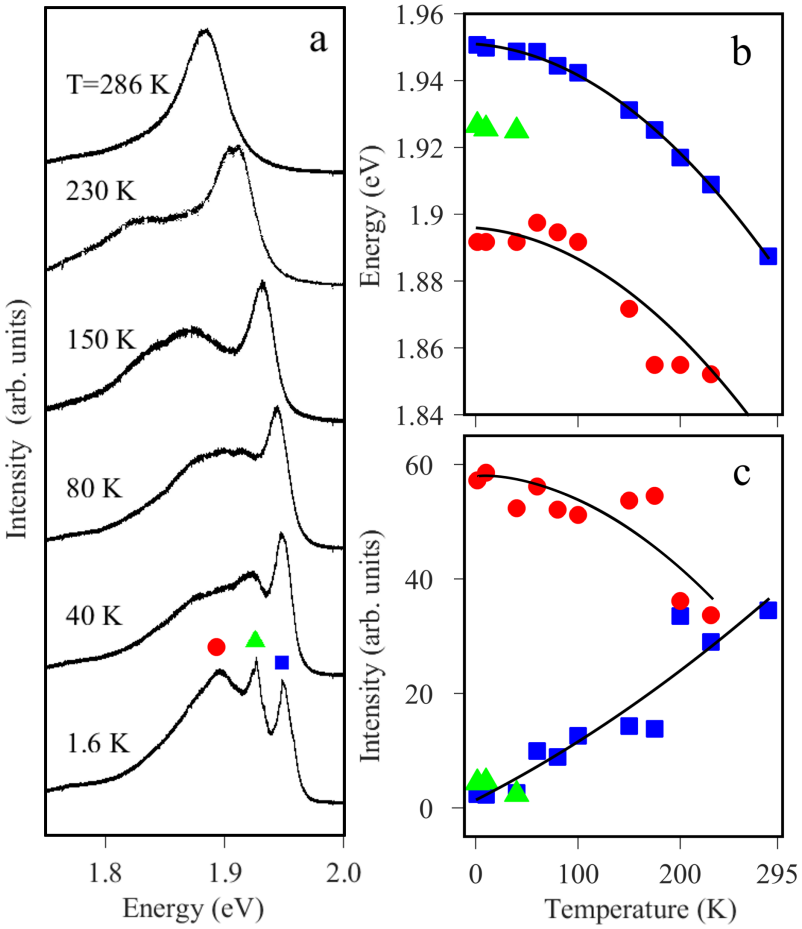

Figure 2.2: Temperature dependence. (a) Emission spectra at different T. The energy (b) and intensity (c) of the emission lines marked in (a) vs. T. The lines are guides to the eye. $P_{\text{ex}} = 0.8\,\text{mW}$, $E_{\text{ex}} = 3.1\,\text{eV}$, $V_g = 0$.

2.2 Results

Figure 2 shows the PL spectra at different temperatures T. At the lowest T, the spectrum consists of two high-energy emission lines with the linewidth $\sim 20\,\text{meV}$ and a broader low-energy line. Additional data and analysis presented below suggest that the high-energy lines correspond to the emission of neutral DXs while the low-energy line to the emission of charged DXs also known as trions.

The energy splitting of 25 meV constitutes only 5% of the MoS_2 exciton binding energy

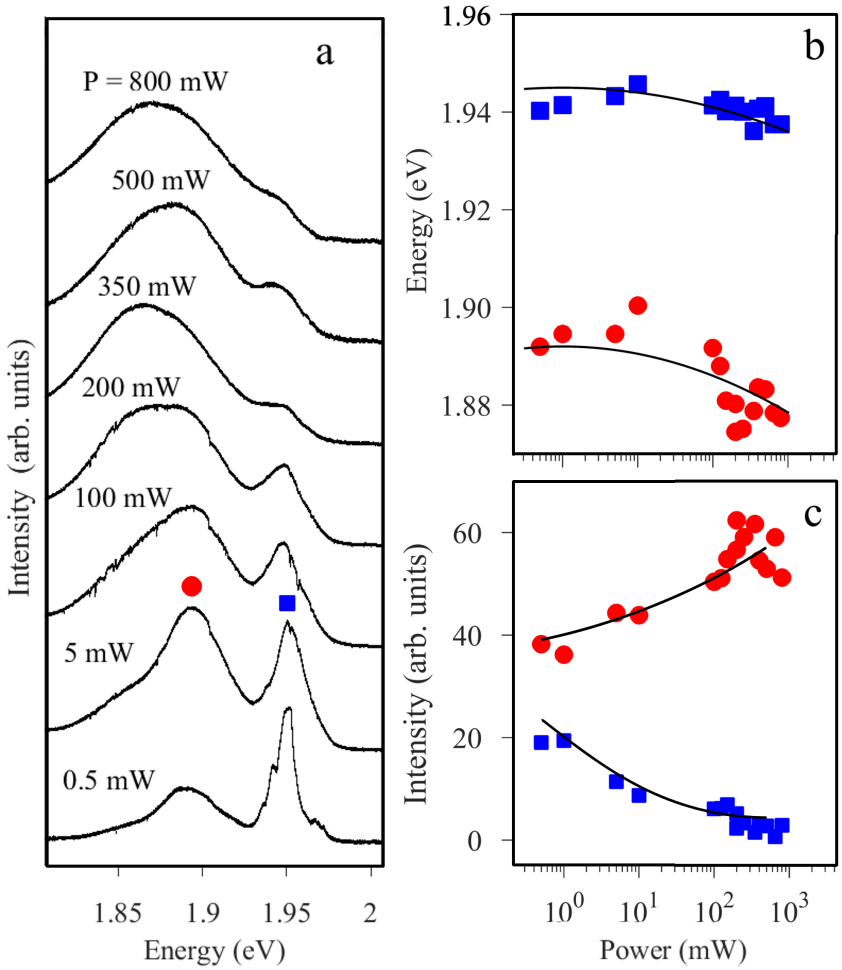

Figure 2.3: Excitation power dependence. (a) Emission spectra at different P_{ex}. The energy (b) and intensity (c) of the emission lines marked in (a) vs. P_{ex}. The lines are guides to the eye. $T = 2\,\mathrm{K}$, $V_g = 0$, $E_{ex} = 2.3\,\mathrm{eV}$.

[16, 17, 21, 22, 23, 24, 25, 29, 31] of about 0.5 eV. It is also much smaller than 0.2 eV energy difference of the A and B excitons [12] caused by the spin-orbit splitting of the valence band (see Figure 4c). These data indicate that the high-energy lines represent different species of A excitons. They can be A excitons with different electron spin states. The calculated 10% difference [41] in the masses, 0.44 vs. $0.49m_0$, of the conduction band spin states results in a 5% difference in the reduced electron-hole masses and, in turn, exciton binding energies. This leads to the energy splitting ~ 25 meV consistent with the experiment.

It is worth noting that the two MoS_2 layers in the structure have inequivalent dielectric environment (Figure 1). This may lead to the difference in the binding energy of excitons in these layers in the effective mass approximation [42]. However, experimental and theoretical studies show that the TMD excitonic states with large binding energy are robust to environmental perturbations [24], meaning the exciton energy is the same for the two MoS_2 layers in the structure.

The lower-energy emission line is shifted by about 50 meV from the first two (Figure 2). This shift is in the range, 20–50 meV, of trion binding energies reported [14, 19, 20, 21] for monolayer MoS_2. The relative intensity of the high-energy exciton lines increases with T (Figure 2), which is consistent with thermal dissociation of trions. The observed red shift of the lines with increasing temperature originates from the band gap reduction, which is typical in semiconductors,[43] the TMDs included [44, 20, 45, 29].

Figure 3 shows the dependence of the exciton PL on the excitation power P_{ex}. The relative intensity of the trion line increases with P_{ex} (Figure 3). This effect may be due to an enhanced probability of trion formation at larger carrier density. A similar increase of the trion PL intensity relative to the exciton was observed in earlier studies of GaAs CQW structures [46].

Figure 4 shows that the polarization of exciton emission can be controlled by the helicity of optical excitation. For a circularly polarized excitation nearly resonant with the exciton line, a high degree of circular polarization $\sim 30\%$ of exciton PL is observed (Figure 4a,b) which is consistent with previous work [13, 14, 15, 18, 26]. This observation indicates that the spin relaxation time is long compared to the exciton recombination and energy relaxation times [47]. The conventional explanation for the slow spin relaxation of excitons invokes spin-orbit coupling (SOC) and spin-valley coupling effects. As illustrated in Figure 4c, the SOC splits valence band of the MoS_2 monolayers, leading to the appearance of the aforementioned A and B exciton states. The B excitons are ~ 0.2 eV higher in energy and their contribution to the PL is negligible. The A excitons can come from either K or K′ valley. It is important however

that the spin and valley indices are coupled, so that exciton spin relaxation requires inter-valley scattering (Figure 4c). If this scattering is weak, the spin relaxation can be long. Virtually no circular polarization is observed for nonresonant optical excitation (Figure 4b), indicating that the high-energy photoexcited carriers loose their spin polarization during energy relaxation. Our time-resolved PL measurements revealed that the exciton and trion lifetimes are short, shorter than the 0.25 ns resolution of the photon counting system. Such small lifetimes facilitate the realization of the regime where the spin relaxation time is long compared to the exciton recombination time, and therefore, the polarization of exciton emission remains high.

Figure 5 shows the gate-voltage dependence of the exciton PL. The small exciton lifetime < 0.25 ns indicates the direct regime in the studied range of voltage because the IX lifetimes are expected to be in the ns range. [40, 30, 27, 32] The positions of the exciton lines remain essentially unchanged while the trion line exhibits a red shift with the slope $\lesssim 0.3$ meV per 1 V of V_g. The smallness of the shifts of the lines corroborates the conclusion that the CQW is in the direct regime. Indeed, if we assume that the electric field in the device is uniform, the IX energy shift with voltage should be $\delta E_{\rm IX}/V_g = eFd/V_g \sim 10\,{\rm meV/V}$. The main effect of the gate voltage in the direct regime is the control of the exciton and trion PL intensities: the high-energy exciton emission increased at negative V_g, while the low-energy trion emission increased at positive V_g (Figure 5). This behavior is explained by the voltage-dependent electron concentration n_e in the MoS_2 layers. The initial electron concentration n_0 at $V_g = 0$ arises from unintentional dopants typically present in MoS_2 materials. The change $\Delta n_e = n_e(V_g) - n_0$ of n_e as a function of V_g can be estimated from simple electrostatics. Treating the CQW as a single unit and neglecting a minor contribution from quantum capacitance, we find

$$\Delta n_e = \frac{C_a R_a - C_b R_b}{R_a + R_b} \frac{V_g}{e}, \tag{2.1}$$

where $C_{a,b}$, $R_{a,b}$ are the geometric capacitances and leakage resistances of the dielectrics above

(below) this double layer. (Incidentally, the leakage current across the device did not exceed a few μA until an eventual breakdown of the device at $V_g \sim 70\,\mathrm{V}$.) Since generally $C_a R_a \neq C_b R_b$, the applied voltage changes n_e and, as a result, modifies the concentration of trions relative to neutral excitons.

2.3 Experiment Setup

The excitons were generated by continuous wave (cw) semiconductor lasers with excitation energies $E_{\mathrm{ex}} = 3.1$, 2.3, or 1.96 eV focused to a spot of diameter $\sim 5\,\mu$m (the circle in Figure 1b). The photoluminescence (PL) spectra were measured using a spectrometer with resolution 0.2 meV and a CCD. In time-resolved PL measurements excitons were generated by a pulsed semiconductor laser with $E_{\mathrm{ex}} = 3.1\,\mathrm{eV}$ and the emitted light was diffracted by the spectrometer and detected by a photomultiplier tube and time correlated photon counting system. The measurements were performed in a ^{4}He cryostat.

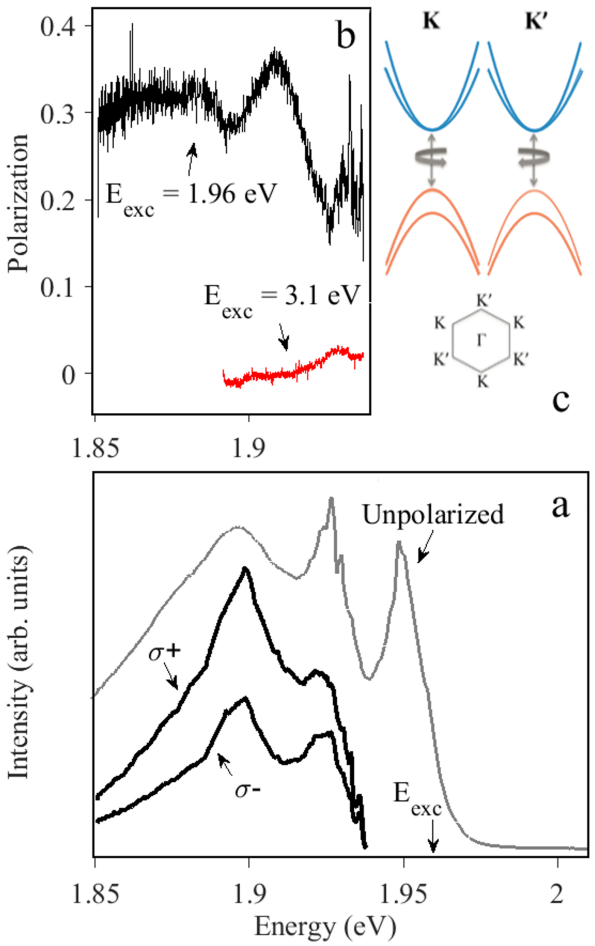

Figure 2.4: Emission polarization. (a) Emission spectra in σ^+ and σ^- polarizations. The laser excitation is σ^+ polarized, $P_{ex} = 0.8\,\mathrm{mW}$, $T = 2\,\mathrm{K}$, $V = 0$, $E_{ex} = 1.96\,\mathrm{eV}$. An unpolarized spectrum at $P_{ex} = 1\,\mathrm{mW}$, $T = 2\,\mathrm{K}$, $V = 0$, $E_{ex} = 3.1\,\mathrm{eV}$ is shown for comparison. (b) The emission polarization for low-energy excitation [indicated by an arrow in (a)] $E_{ex} = 1.96\,\mathrm{eV}$ and high-energy excitation $E_{ex} = 3.1\,\mathrm{eV}$. (c) Schematic illustrating the bands, coupling of valley and spin degrees of freedom, and optical transitions.

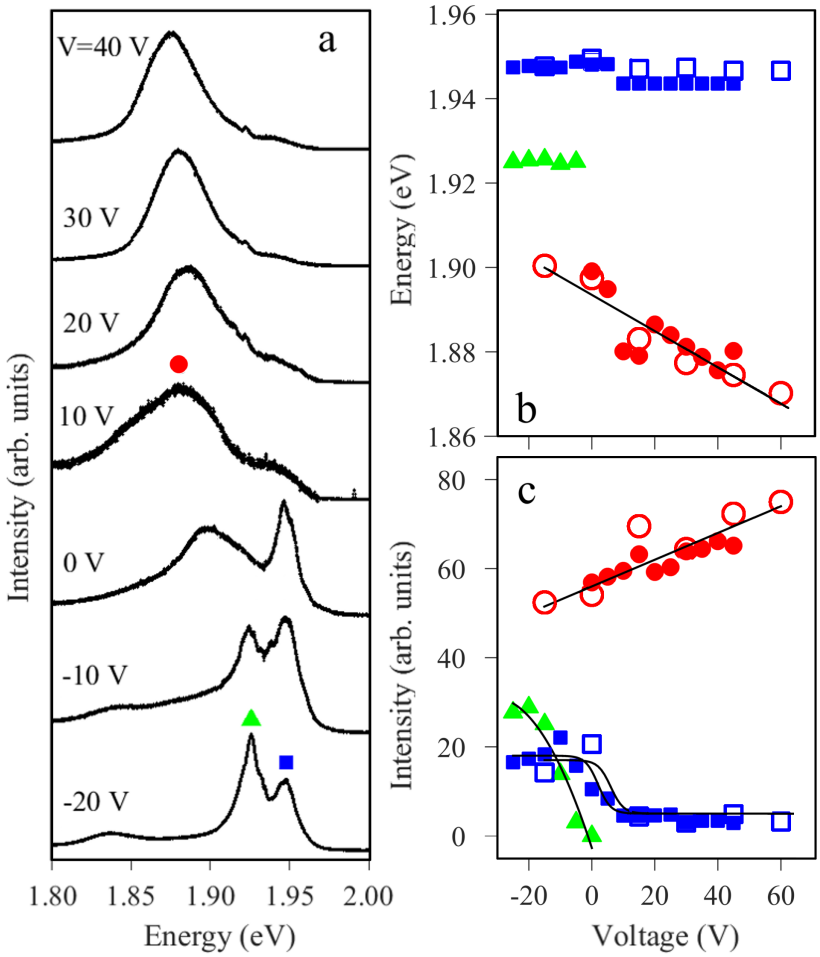

Figure 2.5: Gate voltage dependence. (a) Emission spectra at different V_g. The energy (b) and intensity (c) of the emission lines marked in (a) vs. V_g. The curves are guides to the eye. The solid (open) symbols correspond to $E_{\mathrm{ex}} = 3.1(2.3)\,\mathrm{eV}$, $P_{\mathrm{ex}} = 0.8\,\mathrm{mW}$, $T = 2\,\mathrm{K}$.

Table 2.1: Material parameters of the layers.

Layer	$\varepsilon^{\perp}$	$\varepsilon^{\parallel}$	ε	κ
hBN	6.71	3.56	4.89	1.37
MoS_2	14.29	6.87	9.91	1.44
SiO_2	3.90	3.90	3.90	1.00

2.4 Effective intralayer interaction and exciton binding energy

Here we consider how dielectric environment may effect the binding energy of excitons in a MoS_2 layer in the effective mass approximation. For estimating the binding energies of direct excitons residing in a given MoS_2 layer, we consider a model[29] in which the system consisting of only three layers, labeled top to bottom as $j = 0$, 1, and 2. We treat the MoS_2 layer, which is $j = 1$, as a slab of thickness $c = 0.312\,\text{nm}$. The adjacent layers $j = 0$, 2 are assumed to be semi-infinite, see Figure S1(a). All these materials are uniaxial dielectrics with principal values $\varepsilon_j^{\perp}$ and $\varepsilon_j^{\parallel}$ of the dielectric tensors in the directions perpendicular and parallel to the z-axis, respectively. Our choices for these parameters are listed in the second and third columns of Table 1 (see[40, 29, 21] for literature sources). The average permittivity $\varepsilon_j = \left(\varepsilon_j^{\perp}\varepsilon_j^{\parallel}\right)^{1/2}$ and the anisotropy factor $\kappa_j = \left(\varepsilon_j^{\perp}\right)^{1/2}\left(\varepsilon_j^{\parallel}\right)^{-1/2}$ are provided in the last two columns.

Within the effective mass approximation the exciton binding energy E_B is obtained by solving for the ground-state of a 2D particle of mass μ subject to an effective potential $V(r)$. Here μ is equal to the reduced mass of the electron and the hole while r represents their in-plane separation. The standard procedure for computing $V(r)$ involves two steps. First, one finds the interaction potential $ee'V(r,z,z')$ of two point charges e and $e' = -e$ inside the slab as a function of r and their z-axis coordinates z, z' measured from the midplane of the slab. Next, the desired

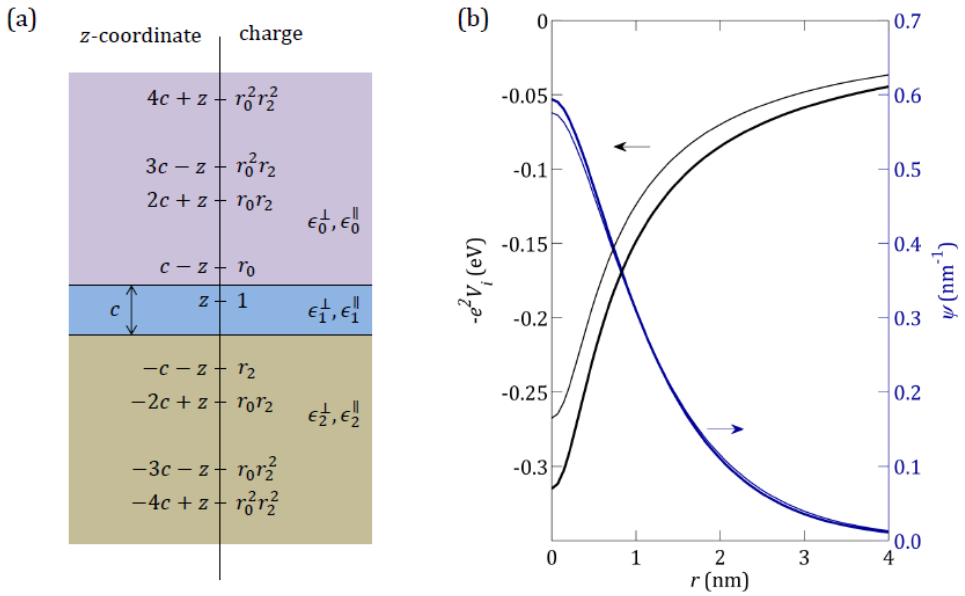

Figure 2.6: Illustration of the model and results. (a) The coordinates and charges of the images due to a unit source charge at z. (b) The image part of the effective potential (left axis) and the internal wavefunction of the exciton (right axis) as a function of the electron-hole distance r. The thin lines are for hBN/MoS_2/hBN, the thick ones are for hBN/MoS_2/SiO_2 structures.

$V(r)$ is obtained by integrating $-e^2V(r,z,z')$ over z and z' with the weight proportional to the squares of the single-particle wavefunctions of the two particles.

The solution of the first problem and its implications for the exciton properties was previously discussed by Keldysh[48] for the case of isotropic media, $\kappa_j = 1$. Recently, Zhang et al.[29] extended his analysis to the uniaxial anisotropy case. We employ an alternative representation of the same potential using the method of images. This representation is more computationally efficient for our simplified calculation in which the Pauli blocking effects[29] are neglected. We write the interaction V of the unit point charges in the form

$$V(r,z,z') = \frac{1}{\varepsilon_1\sqrt{r^2+(z-z')^2\kappa_1^2}} + V_i\,, \tag{2.2}$$

where the leading term represents the "direct" interaction and V_i is the image contribution:

$$V_i(r,z,z') = \sum_{n=0}^{\infty} (r_0 r_2)^n \left(r_0 A_n + r_2 B_n\right), \tag{2.3}$$

$$\begin{aligned} A_n = &\frac{r_2}{\sqrt{r^2 + [(2n+2)c + z - z']^2 \kappa_1^2}} \\ &+ \frac{1}{\sqrt{r^2 + [(2n+1)c - z - z']^2 \kappa_1^2}}, \end{aligned} \tag{2.4}$$

$$\begin{aligned} B_n = &\frac{r_0}{\sqrt{r^2 + [(2n+2)c - z + z']^2 \kappa_1^2}} \\ &+ \frac{1}{\sqrt{r^2 + [(2n+1)c + z + z']^2 \kappa_1^2}}, \end{aligned} \tag{2.5}$$

with

$$r_0 = \frac{\varepsilon_1 - \varepsilon_0}{\varepsilon_1 + \varepsilon_0}, \quad r_2 = \frac{\varepsilon_1 - \varepsilon_2}{\varepsilon_1 + \varepsilon_2} \tag{2.6}$$

being the electrostatic reflections coefficients of 0-1 and 2-1 interfaces. The positions and strengths of the images are illustrated in Figure S1(a).

To model the effect of averaging over z and z' we notice that the characteristic values of these coordinates are some fractions of c. Hence, in the image term V_i they can be in the first approximation neglected. In the direct term, we replace $(z - z')$ by αc, where α is some number less than unity. More generally, α should be considered an adjustable parameter that accounts not only for the thickness of the MoS_2 layer but also for the so-called central-cell correction, that is, short-range exchange and correlation corrections to the electron-hole Coulomb interaction. We

arrive at the effective potential in the form

$$V(r) = -\frac{e^2}{\varepsilon_1\sqrt{r^2+(\alpha\kappa_1 c)^2}} - e^2 V_i(r)\,, \tag{2.7}$$

$$V_i(r) = \sum_{n=0}^{\infty}(r_0 r_2)^n\left[\frac{2r_0r_2}{\sqrt{r^2+[(2n+2)\kappa_1 c]^2}} + \frac{r_0+r_2}{\sqrt{r^2+[(2n+1)\kappa_1 c]^2}}\right]. \tag{2.8}$$

The term $V_i(r)$ can be evaluated analytically in two limits. At $r=0$, it is given by

$$V_i(0) = \sum_{s=\pm 1} s\,\frac{(\sqrt{r_0}-s\sqrt{r_2})^2\ln(1+s\sqrt{r_0}\sqrt{r_2}\,)}{2\varepsilon_1^{\perp}c\sqrt{r_0}\sqrt{r_2}}\,. \tag{2.9}$$

At large r, it becomes Coulombic:

$$V_i(r) \simeq \left(\frac{2}{\varepsilon_0+\varepsilon_2}-\frac{1}{\varepsilon_1}\right)\frac{1}{r}\,, \quad r \gg c\,. \tag{2.10}$$

At intermediate r the series for $V_i(r)$ has to be summed numerically but it poses no difficulty. The results are shown in Figure S1(b) for hBN/MoS_2/hBN and hBN/MoS_2/SiO_2 structures by the thin and thick lines, respectively. In the latter case the electron-hole attraction is stronger, which is consistent with smaller ε (weaker screening) of SiO_2 compared to hBN, see Table 1.

We find the exciton binding energy E_B and internal wavefunction $\psi(r)$ from a numerical solution of the Schrödinger equation

$$\left(-\frac{\hbar^2}{2\mu r}\frac{d}{dr}r\frac{d}{dr}+V(r)+E_B\right)\psi(r)=0 \tag{2.11}$$

discretized on a 300×300 real-space grid.v Note that the reduced electron-hole mass μ is still not accurately known for MoS_2. We use a representative value $\mu = 0.25m_0$ in these calculations[21, 41]. The obtained wavefunctions $\psi(r)$ are shown in Figure S1(b) for the case $\alpha = 0.5$. Due to the

stronger binding potential, $\psi(r)$ for hBN/MoS_2/SiO_2 system is slightly more localized than that for hBN/MoS_2/hBN; otherwise, these wavefunctions are nearly identical, having a characteristic spread of 1 nm each. Note that the asymptotic Coulomb law (2.10) becomes quantitatively accurate only at $r \gtrsim 2$ nm, which is yet another reason why the Rydberg-like formula for E_B cannot be used[21] here (the first reason being a finite α). From our numerical simulations we found that the absolute exciton binding energies do depend on α: $E_B = 216$ meV and 243 meV for $\alpha = 0.1$ vs. $E_B = 267$ meV and 297 meV for $\alpha = 0.5$. The first number in each pair is for hBN/MoS_2/hBN and the second is for hBN/MoS_2/SiO_2. However, the difference of E_B between hBN/MoS_2/hBN and hBN/MoS_2/SiO_2 is approximately the same for both values of α. It is equal to 27 ± 3 meV, with the larger binding energy occurring in the hBN/MoS_2/SiO_2 system.

The presented theoretical analysis is obviously very crude. A more careful calculation could be warranted once accurate values of the basic electronic parameters of the materials in hand are available. One interesting theoretical problem we did not address here at all is a potentially large effect of the frequency and momentum dispersion of the dielectric tensors. Furthermore, accurate estimates require approaches beyond the effective mass approximation considered here. These challenging problems are left for future work. [49]

2.5 Conclusion

In summary, we presented optical studies of excitons in a MoS_2 coupled quantum well van der Waals heterostructure. We observed three emission lines. The dependence of these lines on experimental parameters indicates that the two high energy lines correspond to the emission of neutral excitons and the lowest energy line to the emission of charged excitons (trions). We demonstrated control of the exciton emission by gate voltage, temperature, and also by the helicity and power of optical excitation.

Acknowledgements

Work for this chapter was supported by the U.S. Department of Energy, Office of Basic Energy Sciences under award DE-FG02-07ER46449. M.M.F. was supported by the Office of the Naval Research. Work at the University of Manchester was supported by the European Research Council and the Royal Society.

The text of chapter 2, in part, is a reprint of the material as it appears in E. V. Calman, C. J. Dorow, M. M. Fogler, L. V. Butov, S. Hu, A. Mishchenko, A. K. Geim. Control of excitons in multi-layer van der Waals heterostructures, Appl. Phys. Lett. 108, 101901 (2016) ©, where the dissertation author was the first author. The co-authors in these publications directed, supervised, and co-worked on the research which forms the basis of this chapter.

Author contributions

E.V. Calman, C.J. Dorow, M.M. Fogler, L.V. Butov, S. Hu, A. Mishchenko and A.K. Geim contributed to the work presented in this chapter.

Competing Interests

The authors declare no competing interests.

Chapter 3

Indirect excitons in van der Waals heterostructures at room temperature

Indirect excitons (IXs) are explored both for studying quantum Bose gases in semiconductor materials and for the development of excitonic devices. IXs were extensively studied in III-V and II-VI semiconductor heterostructures where IX range of existence has been limited to low temperatures. Here, we present the observation of IXs at room temperature in van der Waals transition metal dichalcogenide (TMD) heterostructures. This is achieved in TMD heterostructueres based on monolayers of MoS_2 separated by atomically thin hexagonal boron nitride. The IXs we realize in the TMD heterostructure have lifetimes orders of magnitude longer than lifetimes of direct excitons in single-layer TMD and their energy is gate controlled. The realization of IXs at room temperature establishes the TMD heterostructures as a material platform both for a field of high-temperature quantum Bose gases of IXs and for a field of high-temperature excitonic devices.

3.1 Introduction to Indirect Excitons in TMD

An indirect exciton (IX) is composed of an electron and a hole confined in spatially separated quantum well layers. Long lifetimes of IXs allow them to cool below the temperature of quantum degeneracy giving the opportunity to create and study quantum Bose gases in semiconductor materials [50, 51]. Furthermore, IXs are explored for the development of excitonic devices with energy-efficient computation and seamless coupling to optical communication [1]. IXs were extensively studied in III-V and II-VI semiconductor heterostructures. However, their range of existence has been limited so far to low temperatures due to low IX binding energies in these materials. IXs in van der Waals transition-metal dichalcogenide (TMD) heterostructures [52] are characterized by high binding energies making them stable at room temperature and giving the opportunity for exploring high-temperature quantum Bose gases in materials and for creating excitonic devices operational at room temperature, the key for the development of excitonic technology [40, 24, 25].

Experimental studies of quantum degenerate Bose gases of IXs were performed so far in GaAs coupled quantum well (CQW) structures where quantum degeneracy was achieved in the temperature range of few Kelvin. The findings include spontaneous coherence and condensation of excitons [39], long-range spin currents and spin textures [39], spatially modulated exciton state [53], and perfect Coulomb drag [54]. Furthermore, IX energy, lifetime, and flux can be controlled by voltage that is explored for the development of excitonic devices. Excitonic devices with IXs were demonstrated so far at temperatures below ~ 100 K. These devices include traps, lattices, conveyers, and ramps, which are used for studying basic properties of cold IXs, as well as excitonic transistors, routers, and photon storage devices, which hold the potential for creating excitonic signal processing devices and excitonic circuits, a review of excitonic devices can be found in [1].

A finite exciton binding energy E_{ex} limits the operation temperature of excitonic devices.

Excitons exist in the temperature range roughly below E_{ex}/k_B (k_B is the Boltzmann constant) [55]. Furthermore, the temperature of quantum degeneracy, which can be achieved with increasing density before excitons dissociation to electron-hole plasma, also scales proportionally to E_{ex} [40]. These considerations instigate the search for material systems where IXs have a high binding energy and, as a result, can provide the medium for the realization of high-temperature coherent phenomena and excitonic devices.

IXs were explored in various III-V and II-VI semiconductor QW heterostructures based on GaAs [51, 39, 6, 53, 54, 1, 55, 33, 56], AlAs [34, 57], InGaAs [35], GaN [58, 8, 9], and ZnO [59, 7]. Among these materials, IXs are more robust in the ZnO structures where their binding energy is about 30 meV [59]. Proof of principle for the operation of IX switching devices was demonstrated at temperatures up to $\sim$ 100 K in AlAs/GaAs CQW [57] where the IX binding energy is about $\sim$ 10 meV [34]. Studies of IXs in III-V and II-VI semiconductor materials continue to attract intense interest.

Van der Waals structures composed of atomically thin layers of TMD offer an opportunity to realize artificial materials with designable properties, forming a new platform for studying basic phenomena and developing optoelectronic devices [52]. TMD heterostructures allow IXs with remarkably high binding energies [40, 24, 25], much higher than in III-V or II-VI semiconductor heterostructures. Therefore, IXs in TMD heterostructures open the opportunity to realize room-temperature excitonic devices and explore high-temperature quantum degenerate Bose gases of IXs.

The experimental approaches to the realization of IXs in TMD materials involve two kinds of heterostructures. In type I TMD heterostructures with direct gap alignment, the electron and hole layers are spatially separated by a barrier layer. Such type I structures with MoS_2 forming the QW layers and a hexagonal boron nitride (hBN) forming the barrier were considered in [40, 60]. These heterostructures are similar to GaAs/AlGaAs CQW heterostructures where GaAs forms QW layers and AlGaAs forms the barrier [51, 39, 6, 53, 54, 1, 55, 33, 56]. In type

II TMD heterostructures with staggered band alignment, the electron and hole layers form in different adjacent TMD materials such as single-layer $MoSe_2$ and WSe_2 [30, 61, 62, 63], MoS_2 and WSe_2 [27, 64], MoS_2 and WS_2 [65, 32], $MoSe_2$ and WS_2 [66], and MoS_2 and $MoSe_2$ [67]. These heterostructures are similar to AlAs/GaAs CQW heterostructures where electrons and holes are confined in adjacent AlAs and GaAs layers, respectively [34, 57].

Here, we report on the realization of IXs in TMD heterostructures at room temperature. This was achieved using the previously demonstrated approach with MoS_2/hBN type-I CQW [60] combined with an improved structure design and detected using time-resolved optical spectroscopy.

The structure studied here was assembled by stacking mechanically exfoliated two-dimensional crystals on a graphite substrate, which acts as a global backgate (Fig. 1a). The top view of the device showing the contours of different layers is presented in Fig. 1c. The CQW is formed where the two MoS_2 monolayers, separated by three hBN layers, overlap. IXs are formed from electrons and holes in different MoS_2 layers (Fig. 1b). The top and bottom 5 nm thick hBN serve as dielectric cladding layers. Voltage V_g applied between the top graphene layer and the backgate is used to create the bias across the CQW structure. The thickness of hBN cladding layers is much smaller than in our previous CQW TMD device [60]. This allowed us to achieve a much higher electric field across the structure for the applied voltage and, in turn, realize effective control of IX energy by voltage as described below.

3.2 Results

Long Lifetime Emission: IXs dominate the emission spectrum measured after the laser excitation pulse (Fig. 2). At the time delays exceeding the DX recombination times, most of DXs have recombined, and so the recombination of IXs, which have a much longer lifetime, is not masked by the DX recombination. Both short-lifetime DX and long-lifetime IX emission

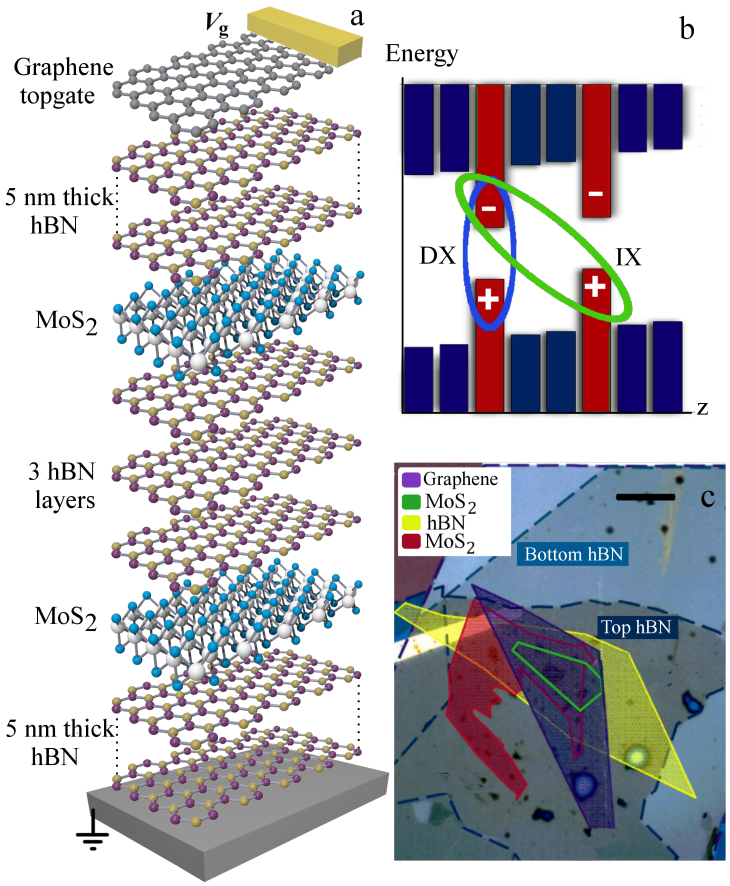

Figure 3.1: The coupled quantum well van der Waals heterostructure layer (a) and energy-band (b) diagrams. The ovals indicate a direct exciton (DX) and an indirect exciton (IX) composed of an electron ($-$) and a hole ($+$). (c) Microscope image showing the layer pattern of the device, scale bar is 10 μm.

lines are observed in the spectrum measured in the time-window between the laser pulses and the first ≈ 2 ns of the laser pulse (Fig. 2). As the fraction of time corresponding to the laser pulse grows, the relative intensity of the DX emission increases. In the cw regime, where the laser is permanently on, DXs dominate the spectrum due to their higher oscillator strength (Fig. 2). Supplementary Figure 2 shows similar spectra at 2 K.

The IX emission kinetics is presented in Fig. 3. The time resolution of the experimental system including the pulse generator, the laser, the photomultiplier, and the time correlated photon counting system is approximately 0.5 ns as seen from the laser decay kinetics measured

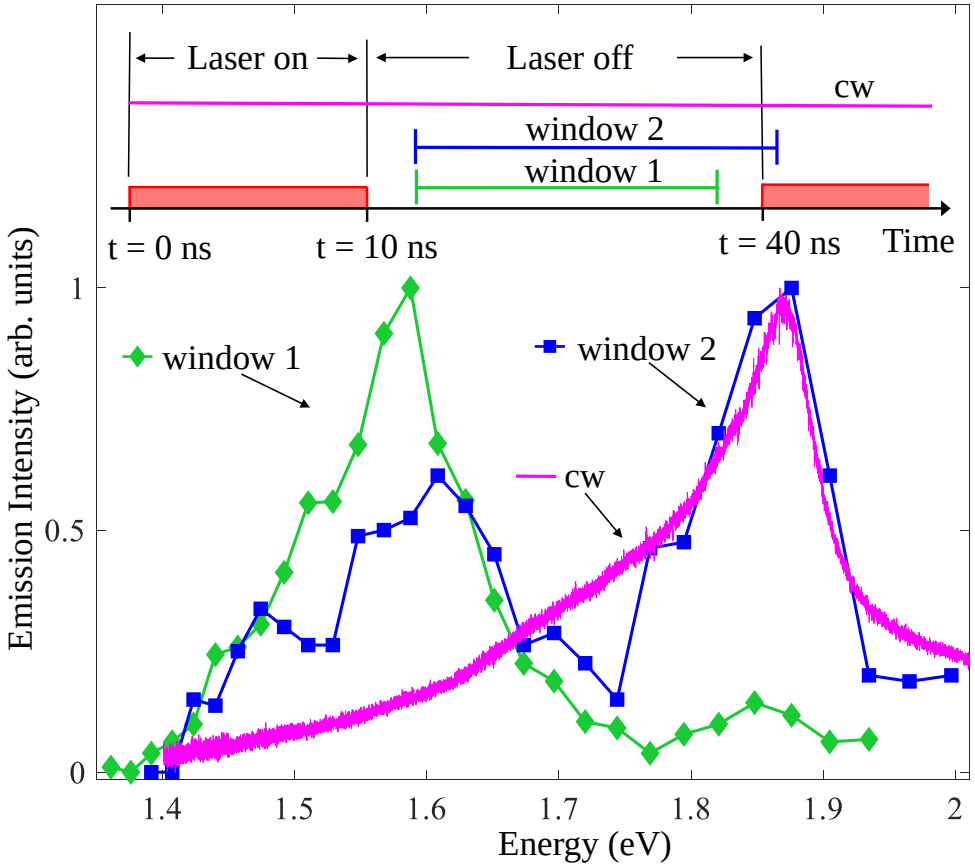

Figure 3.2: Spectrum taken in a time-integration window after the laser pulse (window 1) when most of short-lifetime DXs recombine (green diamonds). The spectrum shows emission of long-lifetime IXs. The laser profile and signal integration windows are shown above. The laser has a pulse duration of 10 ns and a period of 40 ns. Window 2 presents emission from a combination of the laser off and the laser on in a ratio that shows both IX and DX (blue squares). cw spectrum (magenta line) is dominated by direct recombination. $T = 300$ K. $V_g = 0$.

at $E_{ex} = 3.07$ eV. The DX decay kinetics measured at the DX line peak $E_{DX} = 1.89$ eV closely follows the excitation laser decay indicating that the DX lifetime is shorter than the 0.5 ns experimental resolution. The decay kinetics in the IX spectral range $1.46 - 1.65$ eV shows a double-exponential decay (Fig. 3). Its faster component is determined by the decay of low-energy DX states, which appear in the IX spectral range due to the spectral broadening of the DX line, Fig. 2 (similar localized DXs at low energies in the spectral range of IXs were studied in GaAs/AlAs CQW in Ref. [68]). The slower component is determined by the IX decay (Fig. 3).

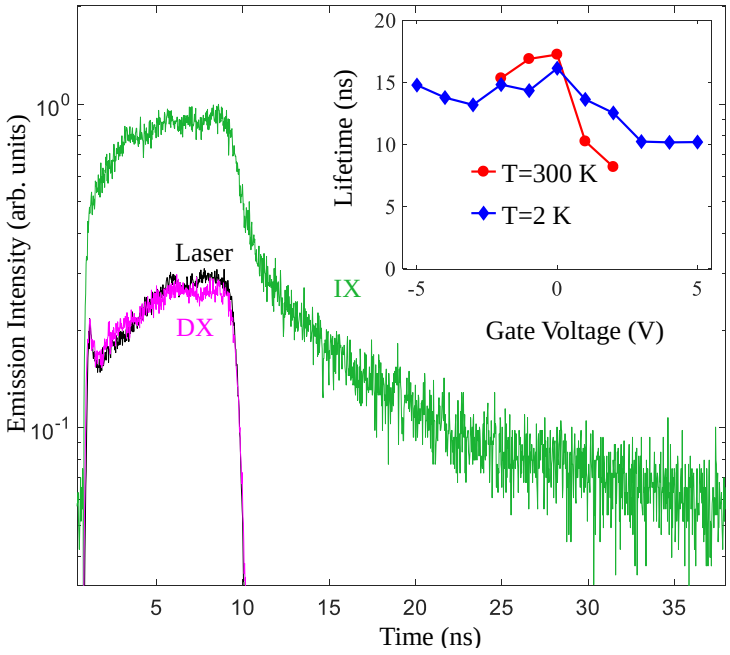

Figure 3.3: Emission kinetics at energies of 1.46–1.65 eV corresponding to the IX spectral range (green), 1.89 eV corresponding to the DX spectral range (magenta), and 3.07 eV corresponding to the excitation laser (black) at $T = 300$ K and $V_g = 0$. IX lifetimes are shown in the inset as a function of gate voltage V_g for $T = 2$ and 300 K, see text. The laser excitation has a pulse duration of 10 ns and a period of 40 ns.

The IX lifetime ~ 10 ns (Fig. 3) is orders of magnitude longer than the DX lifetime [44] and is controlled by gate voltage V_g over a range of several ns (Fig. 3 insert). The voltage dependence of the IX lifetime has two characteristic features. First, it reduces at positive V_g where the IX energy approaches the DX energy (section: "Control of Energy by Voltage"). Second, it has a local maximum around $V_g = 0$ (Supplementary Fig. 1) . Both these features are characteristic of IXs [57]. The former can be attributed to the increase of the overlap of electron and hole wave functions with approaching the direct regime. The latter may result from the suppression of the leakage currents through the CQW layers at zero bias. The realization of the indirect regime, where the IXs are lower in energy than DXs, already at $V_g = 0$ indicates an asymmetry of the device, presumably due to unintenional doping.

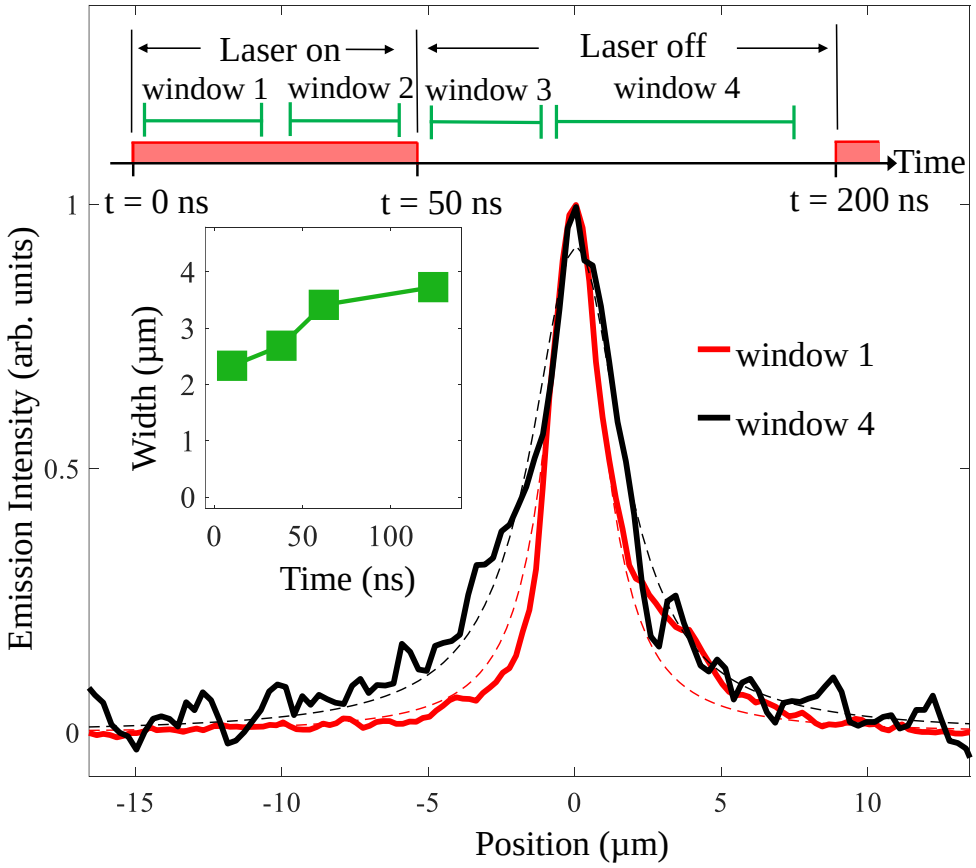

Figure 3.4: Spatial width of the emission at the IX energy 1.46–1.65 eV measured in time windows shown above. The time evolution of the exciton emission width extracted by fitting to lorentzian profiles (dashed lines) is shown in the inset. The excitation laser has a pulse duration of 50 ns and a period of 200 ns. $T = 300$ K. $V_g = 0$.

Transport: Figure 4 shows the spatial profiles of IX emission. The width of the emission profiles determined by a fit to Lorentzian distribution (dashed lines in Fig. 4) is shown in insert to Fig. 4 as a function of time. The emission profiles after the laser excitation pulse have wider spatial distributions than during the pulse. During the laser excitation pulse, the low-energy tail of short-lifetime DX emission strongly contributes to the emission in the IX spectral region (Fig. 2). After the pulse, DXs decay quickly and the emission is dominated by the long-lifetime IXs. Diffusion of IXs away from the laser excitation spot during their long lifetime contributes to the wider spatial profiles of IX emission. The increase in emission width after the pulse end l can

be used for estimating an upper bound on the IX diffusion coefficient D. For $l \sim 1$ μm (Fig. 4) and IX lifetime $\tau \sim 10$ ns (Fig. 3) this gives $D \sim l^2/\tau \sim 1$ cm^2/s.

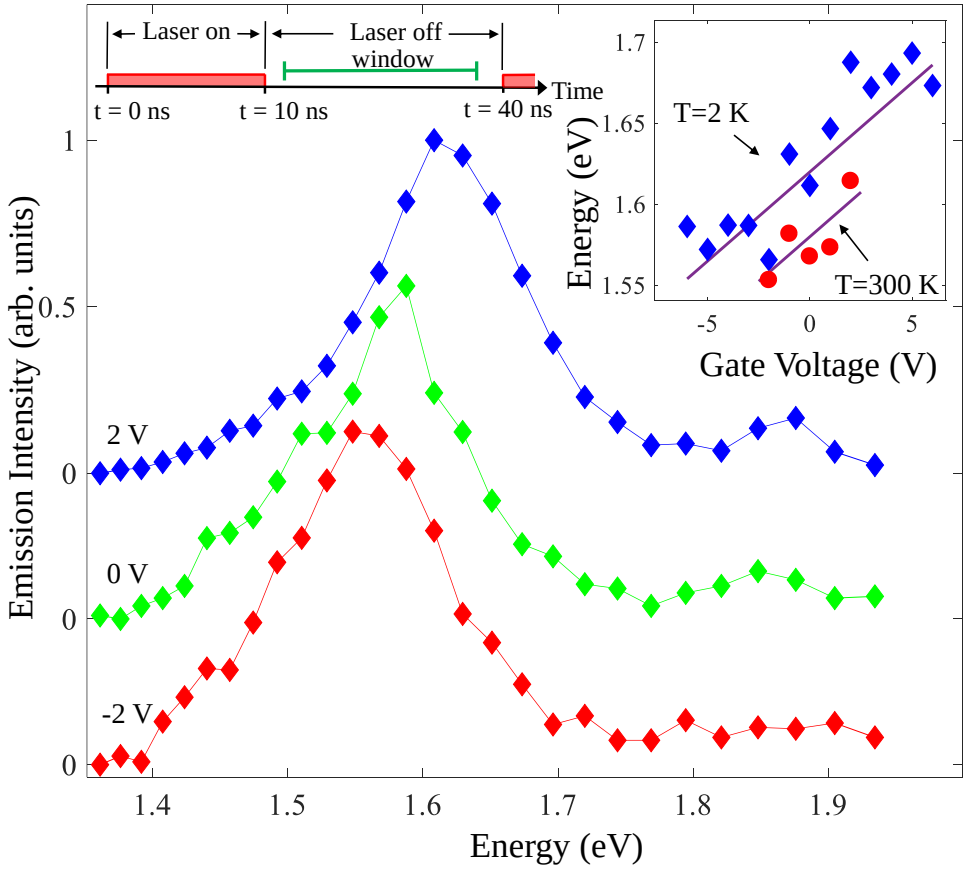

Figure 3.5: Spectra at a delay after the laser excitation pulse in the time window shown above at gate voltages $V_g = -2, 0$, and 2 V at $T = 300$ K. Gate voltage dependence of IX energies at $T = 300$ and 2 K is shown in the insert. The excitation laser has a pulse duration of 10 ns and a period of 40 ns.

Control of Energy by Voltage: Figure 5 shows control of the IX energy by gate voltage. The energy of the long-lifetime emission line shifts by about 120 meV at cryogenic temperatures and by about 60 meV at room temperature. No leakage current or sample damage was detected at cryogenic temperatures in the measurements at applied voltages up to ± 6 V, which is typical for thin hBN that can withstand electric fields of about 0.5 V/nm [69]. However, at room temperature, applying ± 3 V led to the appearance of leakage current through the device and the reduced device

resistivity persisted after lowering V_g. This limited the maximum applied voltage and, in turn, the IX energy shift at room temperature.

3.3 Discussion

Regarding the physical mechanism that governs the IX lifetime in the studied heterostructure we can say the following. In general, this lifetime is limited by tunneling through the hBN spacer. However, direct tunneling across the entire thickness $3 \times 0.33 = 1$ nm of the spacer should be prohibitively slow. The tunneling action and tunneling probability can be estimated to be $S \sim 12$ and $\exp(-2S) \sim 10^{-11}$, respectively, for the potential barrier of height 2 eV and the carrier mass $m_b \sim 0.5$ inside the barrier (similar to [40]). Therefore, we surmise that the IX recombination involves transmission through some midgap defects in the spacer [69] (specific properties of these defects beyond their ability to facilitate tunneling through the hBN layer, relevant to the experiment, are unclear).

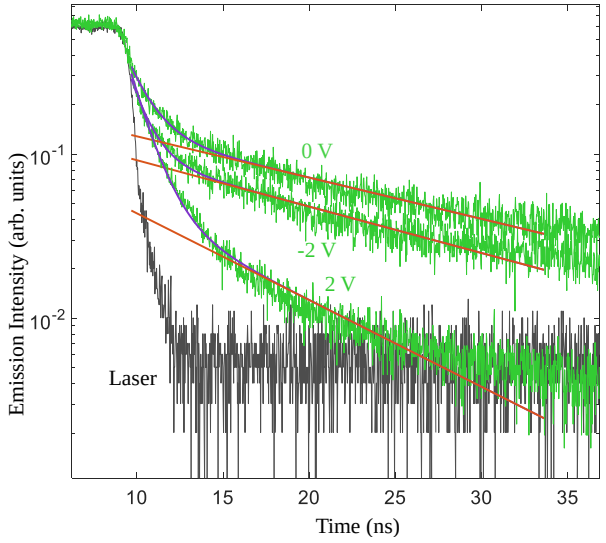

Figure 3.6: Emission kinetics at energies of 1.46–1.65 eV corresponding to the IX spectral range (green) at gate voltages $V_g = -2, 0$, and 2 V at $T = 300$ K. Double exponential fits (blue) and their slower components (red) corresponding to long lifetimes presented in Fig. 3 insert are shown. The laser excitation (black) has a pulse duration of 10 ns and a period of 40 ns.

3.4 Experimental Setup

The excitons were generated by a semiconductor laser with excitation energy $E_{\mathrm{ex}} =$ 3.07 eV. In continuous wave (cw) experiments, photoluminescence (PL) spectra were measured using a spectrometer with resolution 0.2 meV and a liquid-nitrogen-cooled CCD. In all time-resolved experiments, the laser pulses had a rectangular shape with the duration 10–50 ns, period 40–200 ns, and edge sharpness ~ 0.5 ns (Fig. 2). The laser was focused to a ~ 2 μm spot with a power of 0.8 mW. In time-resolved PL kinetics and spectrum measurements, the emitted light was filtered by an interference filter or diffracted by the spectrometer, respectively, and then detected by a photomultiplier tube and time correlated photon counting system. In time-resolved imaging experiments, the emitted light was filtered by an interference filter and detected by a liquid-nitrogen-cooled CCD coupled to a PicoStar HR TauTec time-gated intensifier. The measurements were performed in a ^{4}He atmosphere at room temperature ($T \approx 300$ K) and in a liquid ^{4}He cryostat at 2 K.

Data availability: All relevant data are available from the authors.

3.5 Conclusion

In summary, IXs were observed at room temperature in van der Waals MoS_2/hBN heterostructure. The IXs have long lifetimes, orders of magnitude longer than lifetimes of direct excitons in single-layer MoS_2, and their energy is controlled by voltage at room temperature.

Acknowledgements These studies were supported by DOE Office of Basic Energy Sciences under award DEFG02-07ER46449 and kinetics measurements were supported by NSF Grant No. 1640173 and NERC, a subsidiary of SRC, through the SRC-NRI Center for Excitonic Devices.

The text of chapter 3, in part, is a reprint of the material as it appears in E.V. Calman, M.M. Fogler, L.V. Butov, S. Hu, A. Mishchenko, A.K. Geim. Indirect excitons in van der Waals heterostructures at room temperature, Nature Commun. 9, 1895 (2018). ©, where the dissertation author was the first author. The co-authors in these publications directed, supervised, and co-worked on the research which forms the basis of this chapter.

Author contributions

E.V. Calman, M.M. Fogler, L.V. Butov, S. Hu, A. Mishchenko and A.K. Geim contributed to the work presented in this chapter.

Competing Interests

The authors declare no competing interests.

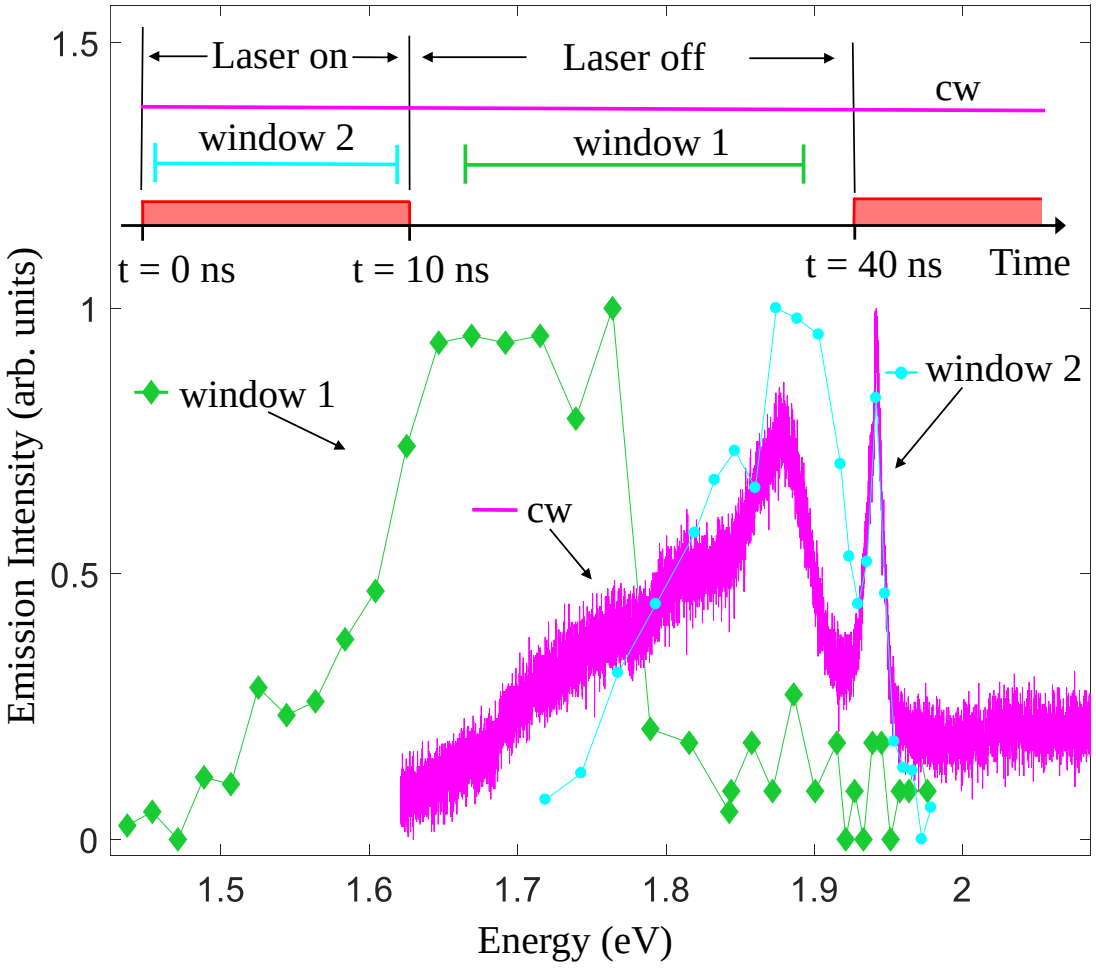

Figure 3.7: Emission spectrum taken in a time-integration window after the laser pulse (window 1) when most of short-lifetime DXs recombine (green diamonds). The spectrum shows emission of long-lifetime IXs. The laser profile and signal integration windows are shown above. The laser has a pulse duration of 10 ns and a period of 40 ns. Emission measured in window 2 during the laser pulse (cyan points) and cw spectrum (magenta line) are dominated by direct recombination. $V_g = -6$ V. $T = 2$ K.

Bibliography

[1] L.V. Butov. Excitonic devices. *Superlattices Microstruct.* 108:2–26, 2017.

[2] K. Sivalertporn, L. Mouchliadis, A. L. Ivanov, R. Philp, and E. A. Muljarov. Direct and indirect excitons in semiconductor coupled quantum wells in an applied electric field. *Physical Review B*, 85(4), jan 2012.

[3] M. Remeika, A. T. Hammack, S. V. Poltavtsev, L. V. Butov, J. Wilkes, A. L. Ivanov, K. L. Campman, M. Hanson, and A. C. Gossard. Pattern formation in the exciton inner ring. *Phys. Rev. B*, 88:125307, Sep 2013.

[4] A. A. High, A. T. Hammack, L. V. Butov, M. Hanson, and A. C. Gossard. Exciton optoelectronic transistor. *Opt. Lett.*, 32(17):2466–2468, Sep 2007.

[5] L. V. Butov and A I. Filin. Energy relaxation and transport of indirect excitons in alas/gaas coupled quantum wells in magnetic field. *Journal of Experimental and Theoretical Physics*, 87:608–611, 09 1998.

[6] A.T. Hammack, J.R. Leonard, S. Yang, L.V. Butov, T. Ostatnický, M. Vladimirova, A.V. Kavokin, T.C.H. Liew, K.L. Campman, A.A. High and A.C. Gossard. Spin currents in a coherent exciton gas. *Phys. Rev. Lett.*, 110:246403, 2013.

[7] Y. Y. Kuznetsova, P. Andreakou, M. W. Hasling, J. R. Leonard, E. V. Calman, L. V. Butov, M. Hanson, and A. C. Gossard. Two-dimensional snowflake trap for indirect excitons. *Optics Letters* 40, 589 (2015)

[8] F. Fedichkin, P. Andreakou, B. Jouault, M. Vladimirova, T. Guillet, C. Brimont, P. Valvin, T. Bretagnon, A. Dussaigne, N. Grandjean and P. Lefebvre Transport of dipolar excitons in (al,ga)n/gan quantum wells. *Phys. Rev. B*, 91:205424, 2015.

[9] F. Fedichkin, T. Guillet, P. Valvin, B. Jouault, C. Brimont, T. Bretagnon, L. Lahourcade, N. Grandjean, P. Lefebvre, and M. Vladimirova Room-temperature transport of indirect excitons in (al,ga)n/gan quantum wells. *Phys. Rev. Applied*, 6:014011, 2016.

[10] A. K. Geim and I. V. Grigorieva. Van der Waals heterostructures. *Nature*, 499(7459):419–425, Jul 2013.

[11] Andrea Splendiani, Liang Sun, Yuanbo Zhang, Tianshu Li, Jonghwan Kim, Chi-Yung Chim, Giulia Galli, and Feng Wang. Emerging photoluminescence in monolayer MoS_2. *Nano Lett.*, 10(4):1271–1275, 2010.

[12] Kin Fai Mak, Changgu Lee, James Hone, Jie Shan, and Tony F. Heinz. Atomically Thin MoS_2: A New Direct-Gap Semiconductor. *Phys. Rev. Lett.*, 105:136805, 2010.

[13] Hualing Zeng, Junfeng Dai, Wang Yao, Di Xiao, and Xiaodong Cui. Valley polarization in MoS_2 monolayers by optical pumping. *Nature Nanotech.*, 7(8):490–493, 2012.

[14] Kin Fai Mak, Keliang He, Jie Shan, and Tony F. Heinz. Control of valley polarization in monolayer MoS2 by optical helicity. *Nature Nanotech.*, 7(8):494–498, 2012.

[15] Ting Cao, Gang Wang, Wenpeng Han, Huiqi Ye, Chuanrui Zhu, Junren Shi, Qian Niu, Pingheng Tan, Enge Wang, Baoli Liu, and Ji Feng. Valley-selective circular dichroism of monolayer molybdenum disulphide. *Nat. Commun.*, 3:887, 2012.

[16] Tawinan Cheiwchanchamnangij and Walter R. L. Lambrecht. Quasiparticle band structure calculation of monolayer, bilayer, and bulk MoS_2. *Phys. Rev. B*, 85(20):205302, 2012.

[17] Ashwin Ramasubramaniam. Large excitonic effects in monolayers of molybdenum and tungsten dichalcogenides. *Phys. Rev. B*, 86(11):115409, 2012.

[18] Sanfeng Wu, Jason S. Ross, Gui-Bin Liu, Grant Aivazian, Aaron Jones, Zaiyao Fei, Wenguang Zhu, Di Xiao, Wang Yao, David Cobden, and Xiaodong Xu. Electrical tuning of valley magnetic moment through symmetry control in bilayer MoS_2. *Nature Phys.*, 9(3):149–153, 2013.

[19] Kin Fai Mak, Keliang He, Changgu Lee, Gwan Hyoung Lee, James Hone, Tony F. Heinz, and Jie Shan. Tightly bound trions in monolayer MoS_2. *Nature Mater.*, 12(3):207–211, 2013.

[20] Jason S. Ross, Sanfeng Wu, Hongyi Yu, Nirmal J. Ghimire, Aaron M. Jones, Grant Aivazian, Jiaqiang Yan, David G. Mandrus, Di Xiao, Wang Yao, and Xiaodong Xu. Electrical control of neutral and charged excitons in a monolayer semiconductor. *Nat. Commun.*, 4:1474, 2013.

[21] Timothy C. Berkelbach, Mark S. Hybertsen, and David R. Reichman. Theory of neutral and charged excitons in monolayer transition metal dichalcogenides. *Phys. Rev. B*, 88:045318, Jul 2013.

[22] Hongliang Shi, Hui Pan, Yong-Wei Zhang, and Boris I. Yakobson. Quasiparticle band structures and optical properties of strained monolayer MoS_2 and WS_2. *Phys. Rev. B*, 87:155304, 2013.

[23] Diana Y. Qiu, Felipe H. da Jornada, and Steven G. Louie. Optical Spectrum of MoS_2: Many-Body Effects and Diversity of Exciton States. *Phys. Rev. Lett.*, 111:216805, 2013.

[24] Ziliang Ye, Ting Cao, Kevin O'Brien, Hanyu Zhu, Xiaobo Yin, Yuan Wang, Steven G. Louie, and Xiang Zhang. Probing excitonic dark states in single-layer tungsten disulphide. *Nature*, 513(7517):214–218, 2014.

[25] A. Chernikov, T. C. Berkelbach, H. M. Hill, A. Rigosi, Y. Li, O. B. Aslan, D. R. Reichman, M. S. Hybertsen, and T. F. Heinz. Non-Hydrogenic Exciton Rydberg Series in Monolayer WS_2. *Phys. Rev. Lett.*, 113:076802, 2014.

[26] Xiaodong Xu, Wang Yao, Di Xiao, and Tony F. Heinz. Spin and pseudospins in layered transition metal dichalcogenides. *Nature Phys.*, 10(5):343–350, 2014.

[27] H. Fang, C. Battaglia, C. Carraro, S. Nemsak, B. Ozdol, J. S. Kang, H. A. Bechtel, S. B. Desai, F. Kronast, A. A. Unal, Giuseppina Conti, Catherine Conlon, Gunnar K. Palsson, Michael C. Martin, Andrew M. Minor, Charles S. Fadley, Eli Yablonovitch, Roya Maboudian, and Ali Javey. Strong interlayer coupling in van der Waals heterostructures built from single-layer chalcogenides. *PNAS*, 111(17):6198–6202, 2014.

[28] Rui Cheng, Dehui Li, Hailong Zhou, Chen Wang, Anxiang Yin, Shan Jiang, Yuan Liu, Yu Chen, Yu Huang, and Xiangfeng Duan. Electroluminescence and photocurrent generation from atomically sharp WSe_2/MoS_2 heterojunction *p-n* diodes. *Nano Lett.*, 14(10):5590–5597, 2014.

[29] Changjian Zhang, Haining Wang, Weimin Chan, Christina Manolatou, and Farhan Rana. Absorption of light by excitons and trions in monolayers of metal dichalcogenide MoS_2: Experiments and theory. *Phys. Rev. B*, 89:205436, 2014.

[30] Pasqual Rivera, John R. Schaibley, Aaron M. Jones, Jason S. Ross, Sanfeng Wu, Grant Aivazian, Philip Klement, Kyle Seyler, Genevieve Clark, Nirmal J. Ghimire, Jiaqiang Yan, D. G. Mandrus, Wang Yao and Xiaodong Xu. Observation of long-lived interlayer excitons in monolayer MoSe2WSe2 heterostructures. *Nat. Commun.* 6:6242, 2015.

[31] Diana Y. Qiu, Felipe H. da Jornada, and Steven G. Louie. Erratum: Optical Spectrum of MoS_2: Many-Body Effects and Diversity of Exciton States [Phys. Rev. Lett. **111**, 216805 (2013)]. *Phys. Rev. Lett.*, 115:119901, 2015.

[32] Maurizia Palummo, Marco Bernardi, and Jeffrey C. Grossman. Exciton Radiative Lifetimes in Two-Dimensional Transition Metal Dichalcogenides. *Nano Lett.*, 15(5):2794–2800, 2015.

[33] M. N. Islam, R. L. Hillman, D. A. B. Miller, D. S. Chemla, A. C. Gossard, and J. H. English. Electroabsorption in GaAs/AlGaAs coupled quantum well waveguides. *Appl. Phys. Lett.*, 50(16):1098, 1987.

[34] A. Zrenner, P. Leeb, J. Schäfer, G. Böhm, G. Weimann, J. M. Worlock, L. T. Florez, and J. P. Harbison. Indirect excitons in coupled quantum well structures. *Surf. Sci.*, 263(1-3):496–501, 1992.

[35] L. V. Butov, A. Zrenner, G. Abstreiter, A. V. Petinova, and K. Eberl. Direct and indirect magnetoexcitons in symmetric $In_xGa_{1-x}As$/GaAs coupled quantum wells. *Phys. Rev. B*, 52:12153–12157, 1995.

[36] Y. E. Lozovik and V. I. Yudson. A new mechanism for superconductivity: pairing between spatially separated electrons and holes. *Sov. Phys. JETP*, 44:389, 1976.

[37] T. Fukuzawa, S.S. Kano, T.K. Gustafson, and T. Ogawa. Possibility of coherent light emission from Bose condensed states of SEHPs. *Surf. Sci.*, 228(1-3):482–485, 1990.

[38] A. A. High, E. E. Novitskaya, L. V. Butov, M. Hanson, and A. C. Gossard. Control of Exciton Fluxes in an Excitonic Integrated Circuit. *Science*, 321(5886):229–231, 2008.

[39] A. A. High, J. R. Leonard, A. T. Hammack, M. M. Fogler, L. V. Butov, A. V. Kavokin, K. L. Campman, and A. C. Gossard. Spontaneous coherence in a cold exciton gas. *Nature*, 483(7391):584–588, 2012.

[40] M. M. Fogler, L. V. Butov, and K. S. Novoselov. High-temperature superfluidity with indirect excitons in van der Waals heterostructures. *Nat. Commun.*, 5:4555, 2014.

[41] Andor Kormányos, Viktor Zólyomi, Neil D. Drummond, and Guido Burkard. Spin-Orbit Coupling, Quantum Dots, and Qubits in Monolayer Transition Metal Dichalcogenides. *Phys. Rev. X*, 4:011034, 2014.

[42] See supplemental material at [URL will be inserted by AIP] for estimates of the exciton binding energies.

[43] Y.P. Varshni. Temperature dependence of the energy gap in semiconductors. *Physica*, 34(1):149–154, Jan 1967.

[44] T. Korn, S. Heydrich, M. Hirmer, J. Schmutzler, and C. Schüller. Low-temperature photocarrier dynamics in monolayer MoS_2. *Appl. Phys. Lett.*, 99(10):102109, 2011.

[45] Ryan Soklaski, Yufeng Liang, and Li Yang. Temperature effect on optical spectra of monolayer molybdenum disulfide. *Appl. Phys. Lett.*, 104(19):193110, 2014.

[46] L. V. Butov, A. Imamoglu, K. L. Campman, and A. C. Gossard. Coulomb effects in spatially separated electron and hole layers in coupled quantum wells. *J. Exp. Theor. Phys.*, 92(2):260–266, 2001.

[47] M. Z. Maialle, E. A. de Andrada e Silva, and L. J. Sham. Exciton spin dynamics in quantum wells. *Phys. Rev. B*, 47:15776–15788, 1993.

[48] L. V. Keldysh. Coulomb interaction in thin semiconductor and semimetal films. *JETP Lett.*, 29:658, 1979.

[49] D. Ballarini, M. De Giorgi, E. Cancellieri, R. Houdré, E. Giacobino, R. Cingolani, A. Bramati, G. Gigli, and D. Sanvitto. All-optical polariton transistor. *Nat. Commun.*, 4:1778, Apr 2013.

[50] Yu. E. Lozovik and V.I. Yudson.

[51] L. V. Butov, A. L. Ivanov, A. Imamoglu, P. B. Littlewood, A. A. Shashkin, V. T. Dolgopolov, K. L. Campman, and A. C. Gossard. Stimulated scattering of indirect excitons in coupled quantum wells: Signature of a degenerate bose-gas of excitons. 86:5608–5611, 2001.

[52] A.K. Geim and I.V. Grigorieva. Van der waals heterostructures. *Nature*, 499:419–425, 2013.

[53] Sen Yang, L. V. Butov, B. D. Simons, K. L. Campman, and A. C. Gossard. Fluctuation Gossard, and commensurability effect of exciton density wave. *Phys. Rev. B*, 91:245302, 2015.

[54] D. Nandi, A. D. K. Finck, J. P. Eisenstein, L. N. Pfeiffer and K. W. West. Exciton condensation and perfect coulomb drag. *Nature*, 488:481–484, 2012.

[55] D. Chemla, D. Miller, P. Smith, A. Gossard, and W. Wiegmann. Room temperature excitonic nonlinear absorption and refraction in GaAs/AlGaAs multiple quantum well structures. *IEEE Journal of Quantum Electronics*, 20(3):265–275, 1984.

[56] A. Alexandrou, J. A. Kash, E. E. Mendez, M. Zachau, J. M. Hong, T. Fukuzawa, and Y. Hase. Electric-field effects on exciton lifetimes in symmetric coupled GaAs/$Al_{0.3}Ga_{0.7}As$ double quantum wells. *Phys. Rev. B* 42:9225-9228, 1990.

[57] G. Grosso, J.Graves, A.T.Hammack, A.A.High, L.V.Butov, M. Hanson and A. C. Gossard. Excitonic switches operating at around 100 K. *Nat. Photonics*, 3:577–580, 2009.

[58] P. Lefebvre, S. Kalliakos, T. Bretagnon, P. Valvin, T. Taliercio, B. Gil, N. Grandjean, and J. Massies. Observation and modeling of the time-dependent descreening of internal electric field in a wurtzite gan/$al_{0.15}ga_{0.85}n$ quantum well after high photoexcitation. *Phys. Rev. B*, 69:035307, 2004.

[59] Bretagnon T. Lefebvre P. Tang X. Valvin P. Guillet T. Gil B. Taliercio T. Teisseire-Doninelli M. Vinter B. Morhain, C. and C. Deparis. Internal electric field in wurtzite zno/$zn_{0.78}mg_{0.22}o$ quantum wells. *Phys. Rev. B*, 72:241305(R).

[60] E. V. Calman, C. J. Dorow, M. M. Fogler, L. V. Butov, S. Hu, A. Mishchenko, and A. K. Geim. Control of excitons in multi-layer van der waals heterostructures. *Appl. Phys. Lett.*, 108:101901, 2016.

[61] Pasqual Rivera, Kyle L. Seyler, Hongyi Yu, John R. Schaibley, Jiaqiang Yan, David G. Mandrus, Wang Yao and Xiaodong Xu. Valley-polarized exciton dynamics in a 2D semiconductor heterostructure. *Science*351, 6274:688-691

[62] Bastian Miller, Alexander Steinhoff, Borja Pano, Julian Klein, Frank Jahnke, Alexander Holleitner and Ursula Wurstbauer. Long-lived direct and indirect interlayer excitons in van der waals heterostructures. *Nano Lett.*, 17:5229–5237, 2017.

[63] Philipp Nagler, Gerd Plechinger, Mariana V Ballottin, Anatolie Mitioglu, Sebastian Meier, Nicola Paradiso, Christoph Strunk, Alexey Chernikov, Peter C M Christianen, Christian Schller. Interlayer exciton dynamics in a dichalcogenide monolayer heterostructure. *2D Mater.*, 4:025112, 2017.

[64] Simone Latini, Kirsten T. Winther, Thomas Olsen and Kristian S. Thygesen. Interlayer Excitons and Band Alignment in MoS_2/hBN/WSe_2 van der Waals Heterostructures. *Nano Lett.* 17:938-945 2017.

[65] Xiaoping Hong, Jonghwan Kim, Su Fei Shi, Yu Zhang, Chenhao Jin, Yinghui Sun, Sefaattin Tongay, Junqiao Wu, Yanfeng Zhang and Feng Wang. Ultrafast charge transfer in atomically thin MoS_2/WS_2 heterostructures. *Nat. Nano.* 9:682-686 2014.

[66] Matthew Z. Bellus, Frank Ceballos, Hsin-Ying Chiu and Hui Zhao. Tightly Bound Trions in Transition Metal Dichalcogenide Heterostructures. *ACS Nano.* 9,6:6459-6464 2015.

[67] Shinichiro Mouri, Wenjing Zhang, Daichi Kozawa, Yuhei Miyauchi, Goki Eda and Kazunari Matsuda. Thermal dissociation of inter-layer excitons in MoS_2/$MoSe_2$ hetero-bilayers. *Nanoscale* 10:8851, 2018.

[68] A. Zrenner, L. V. Butov, M. Hagn, G. Abstreiter, G. Bhm and G. Weimann. Quantum dots formed by interface fluctuations in AlAs/GaAs coupled quantum well structures Phys. Rev. Lett. 72:3382, 1994.

[69] L. Britnell, R. V. Gorbachev, R. Jalil, B. D. Belle, F. Schedin, A. Mishchenko, T. Georgiou, M. I. Katsnelson, L. Eaves, S. V. Morozov, N. M. R. Peres, J. Leist, A. K. Geim, K. S. Novoselov and L. A. Ponomarenko. Field-Effect Tunneling Transistor Based on Vertical Graphene Heterostructures *Science* 335,6071:947-950, 2012.